Synthetic Metals 161 (2011) 586–590

Contents lists available at ScienceDirect

Synthetic Metals

journal homepage: www.elsevier.com/locate/synmet

# Assembly and patterning of ferromagnetic nanoparticles from solution: A novel low-temperature liquid-phase annealing approach

T. Gang[a,*], M. Groen[a], S. Kinge[b], W.J.M. Naber[a], H. Boschker[c], G. Rijnders[c], D.N. Reinhoudt[b], W.G. van der Wiel[a]

[a] NanoElectronics Group, MESA+ Institute for Nanotechnology, University of Twente, Enschede, Netherlands
[b] Laboratory of Supramolecular Chemistry and Technology, MESA+ Institute for Nanotechnology, University of Twente, Enschede, Netherlands
[c] Inorganic Materials Science Group, MESA+ Institute for Nanotechnology, University of Twente, Enschede, Netherlands

ARTICLE INFO

*Article history:*
Received 13 October 2010
Received in revised form 3 December 2010
Accepted 7 December 2010
Available online 15 January 2011

*Keywords:*
Magnetic nanoparticles
FePtAu
Solution annealing
Scanning tunneling microscopy
Spintronics

ABSTRACT

Ferromagnetic $L1_0$-phase FePtAu nanoparticles (5–6 nm) were prepared using a low-temperature, liquid phase annealing approach. The chemically ordered, ferromagnetic $L1_0$-phase onset occurs for annealing temperatures as low as 150 °C. Large uniaxial magnetic anisotropy ($K_u \sim 10^7$ erg/cm$^3$) and a large long-range ordering parameter have been obtained. Significantly, the low-temperature liquid-phase annealing preserves the organic functionalization groups of the nanoparticles. Hence, these nanoparticles are flexible for further assembly and patterning. In addition, we present the assembly of FePt nanoparticles on ferromagnetic substrates with a thin alumina capping layer. This enables us to investigate spin dependent transport through the FePt nanoparticles by scanning tunneling microscopy.



## 1. Introduction

Nano/microparticle based magnetic tunnel junctions (MTJs) have been paid special attention since an enhanced magnetoresistance was observed compared to thin multilayer based magnetic tunnel junctions [1]. In addition, the nanoparticle (NP) based MTJs do not require a well-defined interface between the NPs or between the NPs and the electrodes, whereas conventional MTJs need a well-defined interface between the ferromagnetic contacts and the tunnel barrier in between [1]. The core component of such devices is a monolayer (or a few layers) of magnetic particles embedded in an insulating matrix such as organic ligand molecules or aluminum oxide.

Practically, NP assemblies with small size distribution and shape variation may be implemented in ultra small magnetic devices [2,3]. However, two major challenges still remain. The first challenge is energy and cost efficient production of single-domain particles that are ferromagnetic at room temperature. The second challenge is the reliable assembly of those NPs on a surface.

Chemically synthesized FePt magnetic NPs offer a new possibility to address the first issue. The chemically prepared FePt NPs have high chemical stability, show ferromagnetic behavior up to room temperature, and have a very small size distribution [2]. So far, a major drawback in FePt NP synthesis is the involvement of a high-temperature annealing process (~700 °C and above) to obtain the desired crystal phase with high magnetocrystalline anisotropy [4]. Treatment is generally performed on dried powders, which always leads to particle degeneration, mainly due to the aggregation between the NPs. More importantly, high-temperature treatment destroys the organic ligands surrounding the NPs, which are essential for chemical recognition and self-assembly in monolayers. Several strategies have been applied to avoid agglomeration upon high-temperature treatment. For instance, coating the NPs with thick (10 nm) $SiO_2$ [5], bury the NPs in a salt matrix [6] or a zeolite matrix [7], and recently coating the NPs with MgO [8,9]. Indeed these approaches somewhat prevent the agglomeration. However, high temperature is still necessary and results in the degeneration of the organic ligands, consequently losing all chemical functionality.

Given the above drawbacks, a lower annealing temperature is strongly preferable. Au alloying in low amounts significantly decreases the annealing temperature for transforming the fcc phase to the $L1_0$ phase [10–12]. During the annealing, Au atoms seem to move away from the FePt lattice at relative low temperature, resulting in lattice vacancies and defects, which promote Fe and Pt atoms to rearrange [12–16]. To avoid agglomeration, the NPs can be annealed in a liquid or a solution with a

* Corresponding author at: Nano Electronics Group, MESA+ Institute for Nanotechnology, University of Twente, P.O. Box 217, 7500 AE Enschede, Netherlands.
*E-mail address:* T.Gang@utwente.nl (T. Gang).

0379-6779/$ – see front matter © 2010 Elsevier B.V. All rights reserved.
doi:10.1016/j.synthmet.2010.12.012

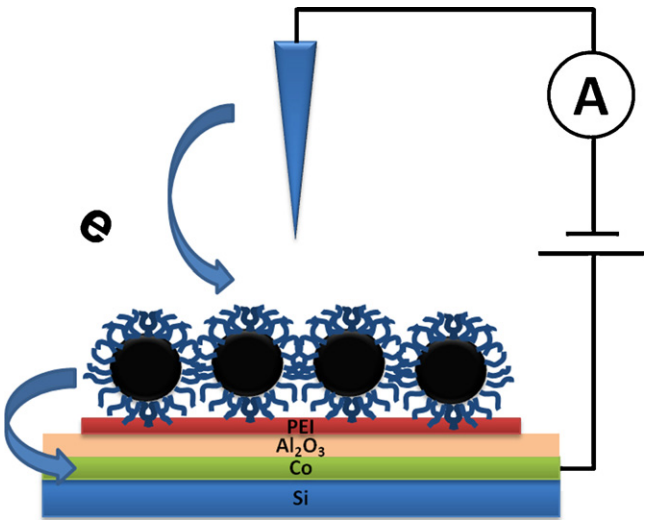


**Scheme 1.** A schematic drawing of a NP based vertical MTJ device.

reduced annealing temperature [12,17]. However, these methods lead to unfavorable increase in particle size or reduce in dispersity.

Here, we carried out a systematic study of low-temperature synthesis in solution that leads to highly uniform, ferromagnetic and chemically patternable FePtAu NPs [17]. Structural analysis indicates a major $L1_0$ phase fraction. Magnetic analysis shows NPs of few nm size remain ferromagnetic at room temperature. At an annealing temperature as low as 150 °C, the $L1_0$ phase sets in. The long-range order parameter $S$ [18] shows a monotonous increase with increasing synthesis temperature. Significantly, our approach leaves the organic ligands surrounding the NPs intact, as demonstrated by monolayer patterning assisted by chemical recognition.

As mentioned before, the second challenge is reliable assembly of the magnetic NPs on a surface. In a previous study, we extended current nanoparticle patterning methods to alumina substrates with controllable coverage [19]. This offers us the possibility to fabricate NPs monolayer based MTJ devices. Subsequently, the spin-dependent electron transport through the NPs can be studied. We applied a scanning tunneling microscopy (STM) based approach to study the transport properties of the NPs. STM is a powerful tool, which offers nanometer resolution in imaging and nanometer precession in tip-specimen separation manipulation. As shown in Scheme 1, the substrate on which NPs are deposited consists of a ferromagnetic (Co) thin film with alumina capping layer. A FePt NP monolayer is assembled on top of the alumina capping layer (Scheme 1). The resulting device forms a MTJ like configuration, which contains two magnetic layers (the Co bottom layer and the NP top layer) with a heterogeneous ($Al_2O_3$/organic) tunnel barrier in between. The STM tip is used as a top contact. This geometry allows us to study nanoscale tunnel magnetoresistance, in particular the interplay with size effects such as Coulomb blockade [20]. We thus synergistically combine inorganic (magnetic) and organic materials, as well as bottom-up (self-assembly) and top-down fabrication methods, being main motivations for organic spintronics [21].

## 2. Experimental details

The NPs were prepared using a modification of the reported procedure by Jia et al. [22]. The synthetic experiments were carried out using standard airless procedures and commercially available reagents. The syntheses were performed by heating the precursors' solution at different temperatures 150 °C, 200 °C, 250 °C, 350 °C for 3 h. At first, a solution of platinum acetylacetonate (0.5 mmol), gold acetate (0.05–0.35 mmol), and 1,2-hexadecanediol (1.5 mmol) in 20-mL octyl ether and 20 mL hexadecylamine was heated up to 100 °C in a three-necked, round-bottom flask under a nitrogen atmosphere. To this solution was added, via syringe, oleic acid (0.5 mmol), oleylamine (0.5 mmol), and iron pentacarbonyl (1 mmol). The mixture was heated to reflux and allowed to reflux for 30 min or 3 h resulting in a black dispersion. Then the heat source was removed and the dispersion was allowed to cool to the room temperature. The inert gas protected solution could then be opened to ambient environment. Adding 40 mL ethanol precipitated the black product. The mixture was centrifuged to isolate the particles from the brown supernatant. The particles were redispersed in hexane, precipitated with ethanol, and isolated by centrifuging. The particles were dried at room temperature in a vacuum oven to give 100–200 mg of particles. The dispersion and precipitation removed impurities. During synthesis, the relative amounts of platinum acetylacetonate and iron pentacarbonyl and gold acetate were fixed in order to produce NPs with similar compositions $(FePt)_{85}Au_{15}$. FePt nanoparticles are prepared according to the same procedure without addition of gold acetate in the reactant mixture.

The substrate of the NPs based MTJ consists of ferromagnetic contacts with alumina capping layer. The alumina capping layer and the ferromagnetic contacts were deposited by e-beam evaporation at a base pressure of $10^{-10}$ mbar. The tunnel barrier was deposited using an Al source, followed by an in situ plasma oxidation step to convert Al to $Al_2O_3$. The thickness of the Al layer is 2 nm and the oxidation time is 30 min. 10 nm of ferromagnetic Co layers were deposited as electrode material. Patterning was done by photo lithography and subsequently the metal lift-off.

FePtAu or FePt NPs monolayers were prepared via polymer mediate self-assembly [2,22]. $O_2$ plasma treated silicon substrates or freshly prepared substrate for NPs based MTJ device were immersed in 20 mg/ml chloroform solution of poly(ethylenimine) (PEI) for 5 min and then dipped in ethanol several times to wash away extra PEI. PEI covered silicon substrates were immersed into FePtAu NPs or FePt NPs (10 mg/ml) hexane solution for 10 min to assemble FePtAu NPs or FePt NPs on the surfaces. Then the substrates were rinsed with pure hexane to wash off physisorbed particles subsequently dry under $N_2$ flow.

FePtAu NPs monolayer patterns are prepared as follows. Patterns on the photoresist film were prepared using hexamethyldisilazane (HMDS) modified silicon substrate via standard photolithography. The lithographic defined substrate was immersed into FePt (10 mg/ml) hexane solution for 10 min to assemble FePtAu NPs on the surfaces. Then the substrates were rinsed with pure hexane to wash off physisorbed particles. Finally, the substrate was rinse thoroughly with acetone until all the photo resist was removed.

Transmission electron microscopy (TEM) images of NPs were recorded with a Philips CM-30 Twin operating at 200 kV. A drop of hexane solution of the NPs was deposited on the carbon-coated copper grid and allowing the solvent to slowly evaporate. The average NP size is determined averaging over 150 NPs from different frames of TEM images.

The NP sample was analyzed by powder X-ray diffraction (XRD) analysis using a Philips X'Pert diffractometer ($CuK_\alpha$ $\lambda = 1.5418$ Å).

Magnetic hysteresis curves were then recorded in a Quantum Design vibrating sample magnetometer (VSM). This gives information about the phase transformation and ferromagnetic behavior with field up to 9 T and temperature between 5 K and 300 K.

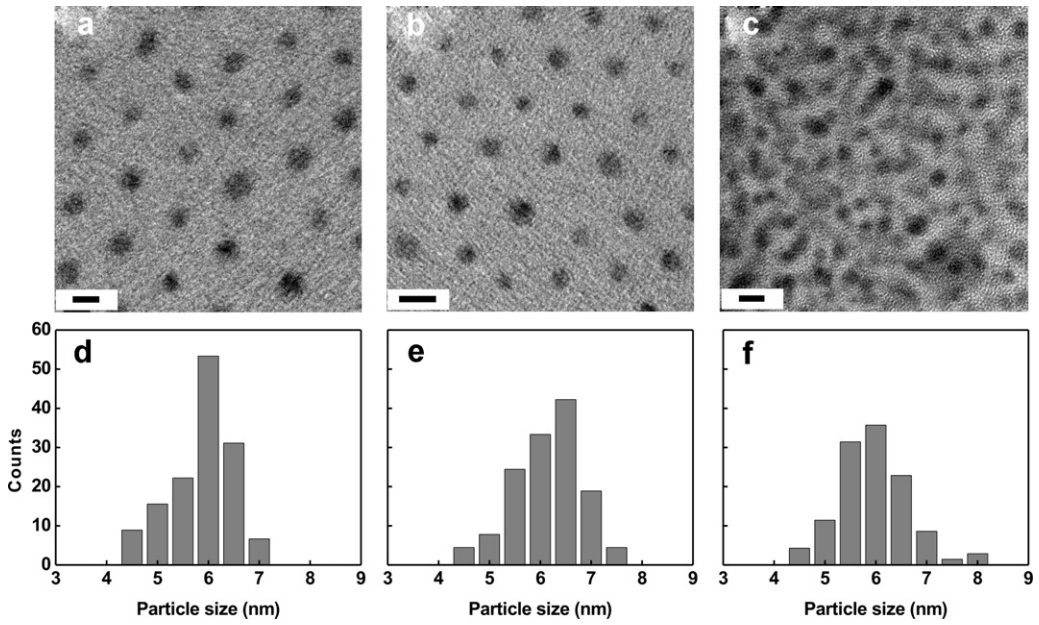


**Fig. 1.** TEM micrographs of $(FePt)_{85}Au_{15}$ NPs prepared under different conditions: (a) 150 °C, 30 min; (b) 200 °C, 3 h; (c) 350 °C, 3 h. The scale bar is 10 nm. (d), (e) and (f) particle size distributions determined from TEM micrographs (a), (b) and (c), respectively [17].

## 3. Results and discussion

For the FePtAu NP preparation, a combination of oleic acid and oleyl amine is used as stabilizing agent for FePtAu NPs. The formation of the NPs is based on the decomposition of iron pentacarbonyl and the reduction of platinum acetylacetonate and gold acetate by a diol in high-temperature solutions. A mixture of octyl ether and hexadecylamine is chosen as solvents. The addition of octyl ether as a solvent is considered essential in our case, which is different from the original method described by Jia et al. Octyl ether is liquid and hexadecylamine is solid at room temperature. This mixture makes sure the metal precursors dissolve at elevated temperature in octyl ether before the hexadecylamine reaches the melting point. The improvement in mixing conditions is believed to be essential for the small size distribution for our NPs.

The FePtAu NPs were synthesized under five different conditions (150 °C, 30 min; 150 °C, 3 h; 200 °C, 3 h; 250 °C, 3 h; 350 °C, 3 h). Fig. 1 shows TEM micrographs of $(FePt)_{85}Au_{15}$ NPs prepared for 30 minutes at 150 °C (Fig. 1a), and for 3 h at 200 °C and 350 °C (Fig. 1b and c). The corresponding particle size distributions indicate small size dispersion (±0.3 nm) of the NPs (Fig. 1d–f, respectively).

The NP diameter obtained from both TEM and XRD analysis for different synthesis temperatures and the elementary composition of the NPs obtained from energy dispersive X-ray diffraction (EDX) are shown in Table 1. The NPs prepared at 250 °C and 350 °C have a broader size distribution. The NPs synthesized at 150 °C and 200 °C have a uniform composition, which is close to the molar ratio of the metal precursors. The NPs synthesized at 250 °C and 350 °C have a relative large distribution of Au contents. For instance, NPs (synthesized at 250 °C) with Au content as high as $Fe_{16}Pt_{22}Au_{62}$ and as low as $Fe_{47}Pt_{45}Au_8$ are observed. This indicates the Au atoms segregate from the FePt lattice upon annealing, i.e. Au domains detach from the FePt NPs. This is in agreement with the mechanism suggested above [12–16], and also with the larger size distribution observed for synthesis at the highest temperature.

The XRD analysis shows the evolution of the $L1_0$ phase with increasing synthesis temperature (Fig. 2a). The evolution of the fundamental peak (0 0 2), as well as the superlattice peaks (0 0 1) and (1 1 0), are clearly observed. The development of the Au (1 1 1) peak indicates Au atoms leaving from the FePt lattice. Using the Scherrer relation, the NP diameter is determined from the XRD characterization [24]. These NP diameters are in very good agreement with those determined from the TEM (Table 1).

A long-range ordering parameter $S$ (defined by Eq. (1)) is generally used to quantify the chemical ordering in the NPs [23].

$$S \cong 0.85\left(\frac{I_{001}}{I_{002}}\right)^{1/2}, \quad (1)$$

In Eq. (1), $I_{001}$ and $I_{002}$ are the integrated intensities of the superlattice 0 0 1 and fundamental 0 0 2 peaks in the XRD spectrum. $S$ is zero for a chemically disordered film and unity for perfectly chemically ordered film [25]. $S$ for NPs synthesized at different temperatures are extracted from the XRD data and listed in Table 1. $S$ increases with increasing synthesis temperature, reaching $S = 0.68$ for NPs synthesized at 350 °C. In comparison, a dry annealing at 725 °C for 2 hours in He achieved $S = 0.98$ [10,11]. Here, significant ordering is achieved without much agglomeration at temperatures

**Table 1**
Summary of particle sizes, compositions, anisotropy constant $K_u$ (derived from the Garcia-Otero model [23]) and long-range ordering parameter $S$.

| Sample | 1 | 2 | 3 | 4 | 5 |
|---|---|---|---|---|---|
| Synthesis temp (°C) | 150 | 150 | 200 | 250 | 350 |
| Synthesis time (h) | 0.5 | 3 | 3 | 3 | 3 |
| Diameter (nm) (TEM) | 5.5 ± 0.3 | 6.2 ± 0.3 | 6.4 ± 0.3 | 7.2 ± 0.3 | 5.8 ± 2.3 |
| Diameter (nm) (XRD) | 5.7 ± 0.7 | 6.5 ± 0.2 | 6.2 ± 0.3 | 6.8 ± 0.3 | 5.6 ± 2.7 |
| Particle composition (EDX) | $Fe_{42}Pt_{41}Au_{17}$ | $Fe_{42}Pt_{44}Au_{14}$ | $Fe_{42}Pt_{40}Au_{18}$ | Distributed | 'Distributed |
| anisotropy constant $K_u$ ($10^7$ erg/cm$^3$) | | 1.2 | 2 | 2.3 | 2.7 |
| Ordering parameter $S$ (derived from $K_u$) | | 0.2 | 0.4 | 0.5 | 0.6 |
| Ordering parameter $S$ (XRD) | | 0.2 | 0.39 | 0.5 | 0.7 |

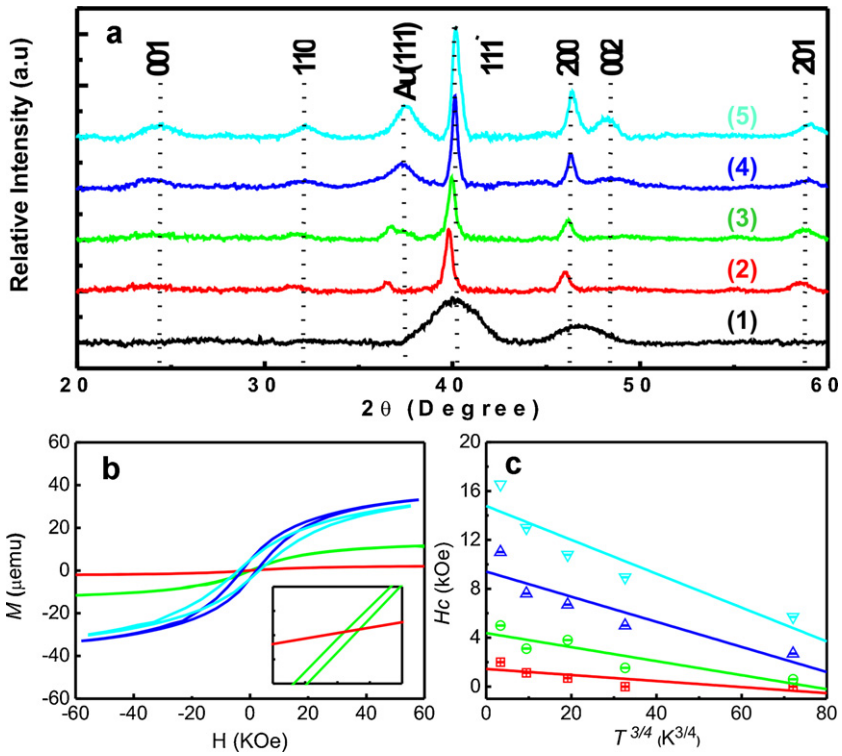


**Fig. 2.** XRD spectra of $(FePt)_{85}Au_{15}$ NPs (a). NP magnetization curves for different synthesis conditions measured by VSM at room temperature (b). The inset of (b) is a zoom in around zero field. The horizontal and vertical axis range is 0.5 kOe and 0.2 μemu, respectively. $H_c$ versus $T^{3/4}$ plots, used for fitting to the Garcia-Otero model, see text (c). In all figures, the curve color refers to the different synthesis conditions: red 150 °C, 3 h; green 200 °C, 3 h; blue 250 °C, 3 h; and cyan 350 °C, 3 h [17]. (For interpretation of the references to color in this figure legend, the reader is referred to the web version of the article.)

less than 350 °C, avoiding ligand degeneration (see below). From 150 °C onwards, the phase transformation starts already for longer synthesis times. This is quite significant since previous reports of dry annealing showed the onset of ordering around 350 °C (30 min) [12–16]. According to Chepulskii et al., the phase transformation of FePt during annealing is kinetically regulated [26,27]. As a result, increasing the refluxing time (from 30 min to 3 h) gives the NPs more time to organize in the desired crystal phase. This is expected to result in the onset of ordering around 150 °C, which is significantly lower compared to previous studies.

Monolayers of FePtAu NPs on silicon/silicon oxide substrate are prepared for magnetic characterization [11,25]. The magnetic properties of NP monolayers are characterized by a vibrating sample magnetometer (VSM) at different measurement temperatures (5–300 K). The hysteresis curves measured at 300 K for NPs prepared at different temperatures are shown in Fig. 2b. From Fig. 2b, hysteresis is obtained for synthesis temperatures 200 °C ($H_c$ = 600 Oe), 250 °C ($H_c$ = 2700 Oe) and 350 °C ($H_c$ = 4800 Oe). This demonstrates room-temperature ferromagnetism of the NPs starting from synthesis temperatures of 200 °C only.

We compare the saturation magnetic moment of the NPs synthesized at 350 °C with the momentum density of bulk FePt (1140 emu/cm$^3$) [28]. In all measurements, our monolayers show a saturation magnetic moment between 35 and 40 μemu. Assuming the ratio of FePt to Au in our FePtAu NPs to be 0.85–0.15, 2.9 nm NP radius and 1 nm ligand length. Based on this information, we derive (see supporting information) a saturation magnetic moment of 47 μemu. The experimentally observation is slightly lower, as expected when taking into account the lower effective packing density and not fully developed $L1_0$ phase.

Our magnetic hysteresis loops show a clear temperature dependence. The coercive fields of the NPs decrease due to increasing thermal fluctuations as the temperature increases. A thermal relaxation model for 2D systems, the Sharrock's formula [29], is widely used for magnetic thin films. Since, our NPs are 3D systems, the magnetic properties of NPs are investigated by the model proposed by Garcia-Otero et al. This model is suitable for magnetically isolated and 3D random particle systems [23]. The expression is

$$\frac{H_c}{H_k} = 0.479 - 0.81\left(\frac{k_B T}{2K_u V}(\ln \tau_m + 20.7)\right)^{3/4} \quad (2)$$

In Eq. (2), $H_k$ is the critical field in Oe, $k_B$ is the Boltzmann constant ($1.38073 \times 10^{-16}$ erg/K), $K_u$ is the uniaxial anisotropy energy density in erg/cm$^3$, $V$ is the particle volume in cm$^3$, and $\tau_m$ is the measurement time in seconds. The magnetic properties of the magnetic NPs can be quantified using this model. Fig. 2c shows the $H_c$ vs. $T^{3/4}$ plots. The fitting may not be perfect but acceptable when compared to other studies [30,31]. According to Eq. (2), $H_k$ can be derived from the intercept of the $H_c$ versus $T^{3/4}$ plots. $K_uV$ can be derived from the slopes of the curves.

The $K_u$ derived from the fits according to Eq. (2) in Fig. 2c are given in Table 1. Based on a measured relationship between anisotropy constants $K_u$ and ordering parameter $S$, $S$ for different synthesis temperatures are obtained (Table 1) [32]. These ordering parameters are in good agreement with the ordering parameters determined by XRD.

Our solution annealed FePtAu NPs have very good dispersity, indicating that the ligands are still intact. The NP monolayer patterns in Fig. 3a is fabricated to demonstrate the post-anneal patterning based on ligand exchange is possible. A thin (0.62 ± 0.04 nm) layer of hexamethyldisilazane (HMDS) was spin coated on $Si/SiO_2$ substrate. Then a pattern is defined by standard photolithography. Subsequently, the substrate was dipped in the NPs dispersion. Pendant functional groups –NH– of the HMDS replace the ligands surrounding the NPs and a stable NP monolayer is formed in the exposed regions. Physisorbed NPs and photoresist are easily washed away afterwards. The successful patterning of the FePtAu NPs based on ligand exchange

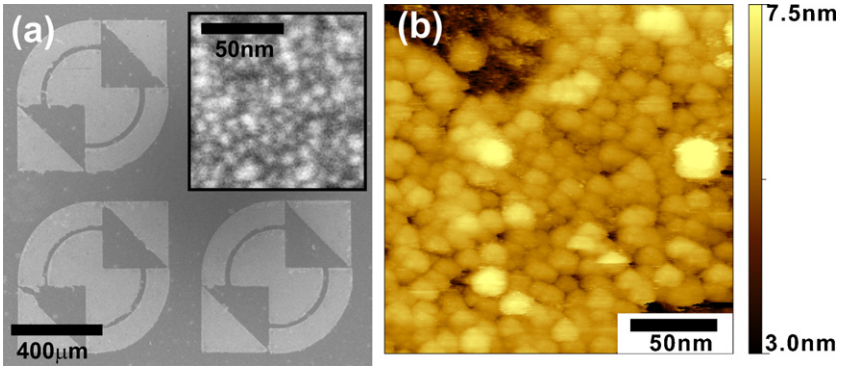


**Fig. 3.** Scanning electron microscope (SEM) images of FePtAu NPs monolayer patterns (a) [17]. The insert shows a zoom in on the patterned area. Topography image of the NPs monolayer assembled on top of the $Al_2O_3$ capping layer obtained by STM (b).

indicates that the ligands are intact after our solution annealing procedure.

A NPs based vertical MTJ device (Scheme 1) is fabricated for studying the possible spin dependent transport property of magnetic NPs. The substrate of the device consists of ferromagnetic Co layer (10 nm) with $Al_2O_3$ capping layer (2 nm) on top. The assembly of FePt NPs on $Al_2O_3$ capping layer mainly consisted of two steps. First activation of freshly made substrate surface by PEI, then ligand exchange between the surfactants around the NPs and the functional groups on the modified $Al_2O_3$ substrate [25]. Normal metallic top electrodes cannot be applied to NP based vertical MTJ devices, since metals penetrate the NP monolayer at defects during metal evaporation. These defects lead to electrical. To overcome this issue, a high-vacuum STM system is used to measure NP based vertical MTJ device. The probe of the STM can approach the top of the NPs without penetrating the NP monolayer. It allows us to study the transport properties of a single NP or a few NPs depend on the packing density of the NP. Fig. 3b is a topography image of the NP monolayer by STM. A densely packed monolayer of FePt NPs is formed on top of the $Al_2O_3$ capping layer. The particle size obtains from the STM measurement is in agreement with the particle size obtained from the TEM. The slight noisy image may attribute to the ligands on NPs. NPs based vertical MTJ device is achieved. This configuration offers a platform to study the spin-dependant transport through NPs.

## 4. Conclusions

In conclusion, we have showed a low-temperature synthesis method in solution for preparing FePtAu NPs that remain ferromagnetic at room temperature. Our method significantly reduces nanoparticle agglomeration and preserves the organic ligands surrounding the NPs. As a result, the post-annealed NPs still have the flexibility for chemical based patterning. Bottom-up synthesis of room temperature ferromagnetic, patternable NPs are considered as an important step towards application of ferromagnetic NPs in spintronics. In addition, we extended current nanoparticle patterning methods to alumina substrates. A geometry for studying NP based vertical MTJ devices is presented. Further work on study the spin-dependant transport through these nanoparticles is currently under way.

## Acknowledgments

We sincerely acknowledge M. Smithers for TEM and EDX analyses. This work is part of WGvdW's VIDI research program 'Organic materials for spintronic devices', financially supported by the Netherlands Organization for Scientific Research (NWO) and the Technology Foundation STW.

## Appendix A. Supplementary data

Supplementary data associated with this article can be found, in the online version, at doi:10.1016/j.synthmet.2010.12.012.

## References

[1] K. Yakushiji, S. Mitani, F. Ernult, K. Takanashi, H. Fujimori, Physics Reports-Review Section of Physics Letters 451 (2007) 1.
[2] S. Sun, C.B. Murray, D. Weller, L. Folks, A. Moser, Science 287 (2000) 1989.
[3] K. Liu, J. Nogues, C. Leighton, H. Masuda, K. Nishio, I.V. Roshchin, I.K. Schuller, Applied Physics Letters 81 (2002) 4434.
[4] I. Zafiropoulou, V. Tzitzios, D. Petridis, E. Devlin, J. Fidler, S. Hoefinger, D. Niarchos, Nanotechnology 16 (2005) 1603.
[5] S. Yamamoto, Y. Morimoto, T. Ono, M. Takano, Applied Physics Letters 87 (2005) 032503.
[6] B.A. Jones, J.D. Dutson, K. O'Grady, B.J. Hickey, D.R. Li, N. Poudyal, J.P. Liu, IEEE Transactions on Magnetics 42 (2006) 3066.
[7] S. Momose, H. Kodama, W. Yamagishi, T. Uzumaki, Japanese Journal of Applied Physics Part 2-Letters & Express Letters 46 (2007) L1105.
[8] J. Kim, C.B. Rong, Y. Lee, J.P. Liu, S.H. Sun, Chemistry of Materials 20 (2008) 7242.
[9] J.M. Kim, C.B. Rong, J.P. Liu, S.H. Sun, Advanced Materials 21 (2009) 906.
[10] S.H. Sun, Advanced Materials 18 (2006) 393.
[11] S.H. Sun, C.B. Murray, D. Weller, L. Folks, A. Moser, Science 287 (2000) 1989.
[12] J.W. Harrell, D.E. Nikles, S.S. Kang, X.C. Sun, Z. Jia, S. Shi, J. Lawson, G.B. Thompson, C. Srivastava, N.V. Seetala, Scripta Materialia 53 (2005) 411.
[13] S.S. Kang, Z.Y. Jia, D.E. Nikles, J.W. Harrell, IEEE Transactions on Magnetics 39 (2003) 2753.
[14] S.H. Kang, Z.Y. Jia, D.E. Nikles, J.W. Harrell, IEEE Transactions on Magnetics 40 (2004) 513.
[15] S. Wang, S.S. Kang, D.E. Nikles, J.W. Harrell, X.W. Wu, Journal of Magnetism and Magnetic Materials 266 (2003) 49.
[16] C.H. Yu, N. Caiulo, C.C.H. Lo, K. Tam, S.C. Tsang, Advanced Materials 18 (2006) 2312.
[17] S. Kinge, T. Gang, W.J.M. Naber, H. Boschker, G. Rijnders, D.N. Reinhoudt, W.G. van der Wiel, Nano Letters 9 (2009) 3220.
[18] B.E. Warren, X-Ray Diffraction; Addison-Wesley Publishing Company: MA, 1969.
[19] O. Yildirim, T. Gang, S. Kinge, D.N. Reinhoudt, D.H.A. Blank, W.G. van der Wiel, G. Rijnders, J. Huskens, International Journal of Molecular Sciences 11 (2010) 1162.
[20] M.H. Devoret, D. Esteve, C. Urbina, Nature 360 (1992) 547.
[21] W.J.M. Naber, S. Faez, W.G. van der Wiel, Journal of Physics D-Applied Physics 40 (2007) R205.
[22] Z.Y. Jia, S.S. Kang, D.E. Nikles, J.W. Harrell, IEEE Transactions on Magnetics 41 (2005) 3385.
[23] J. Garcia-Otero, A.J. Garcia-Bastida, J. Rivas, Journal of Magnetism and Magnetic Materials 189 (1998) 377.
[24] H. Borchert, E.V. Shevehenko, A. Robert, I. Mekis, A. Kornowski, G. Grubel, H. Weller, Langmuir 21 (2005) 1931.
[25] S.H. Sun, S. Anders, T. Thomson, J.E.E. Baglin, M.F. Toney, H.F. Hamann, C.B. Murray, B.D. Terris, Journal of Physical Chemistry B 107 (2003) 5419.
[26] R.V. Chepulskii, W.H. Butler, Physical Review B 72 (2005) 134205.
[27] R.V. Chepulskii, J. Velev, W.H. Butler, Journal of Applied Physics 97 (10) (2005) J311.
[28] T. Klemmer, D. Hoydick, H. Okumura, B. Zhang, W.A. Soffa, Scripta Metallurgica et Materialia 33 (1995) 1793.
[29] D. Weller, A. Moser, IEEE Transactions on Magnetics 35 (1999) 4423.
[30] L.L. Wang, W.T. Zheng, J. Gong, H.B. Li, X. Wang, N. Ma, P.J. Cao, X.C. Ma, Journal of Alloys and Compounds 467 (2009) 1.
[31] J.A. Franco, F.C.e. Silva, Applied Physics Letters 96 (2010) 172505.
[32] T. Shima, T. Moriguchi, S. Mitani, K. Takanashi, Applied Physics Letters 80 (2002) 288.